



## Local approach applied to the fracture toughness of resistance spot welds

Florent Krajcarz, Anne-Françoise Gourgues-Lorenzon, Emmanuel Lucas,  
Matthieu Mazière, André Pineau

### ► To cite this version:

Florent Krajcarz, Anne-Françoise Gourgues-Lorenzon, Emmanuel Lucas, Matthieu Mazière, André Pineau. Local approach applied to the fracture toughness of resistance spot welds. 13th international conference on fracture, Jun 2013, Beijing, China. 10 p. hal-00853411

**HAL Id: hal-00853411**

**<https://hal-mines-paristech.archives-ouvertes.fr/hal-00853411>**

Submitted on 14 Nov 2013

**HAL** is a multi-disciplinary open access archive for the deposit and dissemination of scientific research documents, whether they are published or not. The documents may come from teaching and research institutions in France or abroad, or from public or private research centers.

L'archive ouverte pluridisciplinaire **HAL**, est destinée au dépôt et à la diffusion de documents scientifiques de niveau recherche, publiés ou non, émanant des établissements d'enseignement et de recherche français ou étrangers, des laboratoires publics ou privés.

# Local Approach Applied to the Fracture Toughness of Resistance Spot Welds

**Florent Krajcarz<sup>1,2</sup>, Anne-Françoise Gourgues-Lorenzon<sup>1,\*</sup>, Emmanuel Lucas<sup>2</sup>, Matthieu Mazière<sup>1</sup>, André Pineau<sup>1</sup>**

<sup>1</sup> MINES ParisTech, Centre des Matériaux, UMR CNRS 7633, BP 87, 91003 Evry cedex, France

<sup>2</sup> ArcelorMittal Global R&D, BP 30320, 57283 Maizières-lès-Metz cedex, France

\* Corresponding author: anne-francoise.gourgues@ensmp.fr

**Abstract** A recently developed methodology for measuring the nugget fracture toughness in mode I was applied to three high-strength steel resistance spot welds, exhibiting either mixed cleavage/ductile or ductile fracture at room temperature. Fracture toughness tests revealed a difference in ductile-to-brittle transition temperature between the welds. Constitutive equations of weld nuggets were determined and implemented in a finite element model of the fracture toughness test, revealing both in-plane bending and in-plane stretching in front of the crack tip. Brittle cleavage fracture of the nuggets is not conveniently described using a simple Ritchie-Knott-Rice approach but the Rice-Tracey model allowed quantitatively relating the high number density of small particles to the nugget fracture toughness in the ductile regime.

**Keywords** Local approach, Brittle to ductile transition, High strength steels, Resistance spot welds

---

## 1. Introduction

The need for car-lightening has led to the development of Advanced High Strength Steels containing more alloying elements than standard steels. Resistance spot welding issues become of major concern for these steels. Due to the severe cooling conditions, the weld may exhibit an unusual microstructure that could be sensitive to unstable cracking in opening mode, inducing interfacial failure of the weld. In the opening mode, several tests are available to determine the strength of resistance spot welds (RSWs) [1]. The transition between crack propagation across the heat-affected zone and interfacial failure strongly depends on the molten zone (nugget) fracture toughness [2]. A new methodology (referenced hereafter as UXT tests) has recently been developed [3] to determine the nugget fracture toughness, using cross-tensile tests on double U-shaped specimens (Fig. 1), together with crack extension monitoring using a potential drop method. The purpose of the present study is to determine, if any, the ductile-to-brittle transition of the weld nugget for different steel compositions (and thus, nugget microstructures), by using the UXT test. A mechanical analysis of the test is then performed using a finite element modelling approach to determine the loading conditions ahead of the tip of the precrack. For this purpose, constitutive equations of the nugget are estimated from heat-treated microstructures, as already reported in literature [1]. A simple initiation criterion for both brittle cleavage and ductile dimple fracture is then tentatively derived as a function of the material microstructure and fracture mechanisms.

## 2. Experimental details

### 2.1. Materials and welding conditions

Three high strength steels were provided as 2-mm-thick bare sheets. Their chemical composition and room temperature properties are reported in Table 1. Resistance spot welds were fabricated using a Sciaky pedestal welding machine, following ISO 18278-2 (2004) standard parameters, without cold times. A low welding current (Table 2) was applied (i) to ensure the presence of a weak Diffusion Bonded Zone (DBZ), which serves as an circular precrack, and (ii) to facilitate interfacial failure under UXT tests [2]. The corresponding weld diameter,  $d$  was measured from fracture surfaces after interfacial failure (Table 2). Conventional cross-tensile strength,  $CTS$

(averaged over four tensile tests on cross-welded 125x38 mm<sup>2</sup> coupons), hardness (average of 30 measurements at room temperature with a dwell time of 10s) and nugget microstructure (observed in cross-section after Béchét-Beaujard + Nital etching) are reported in Table 2.

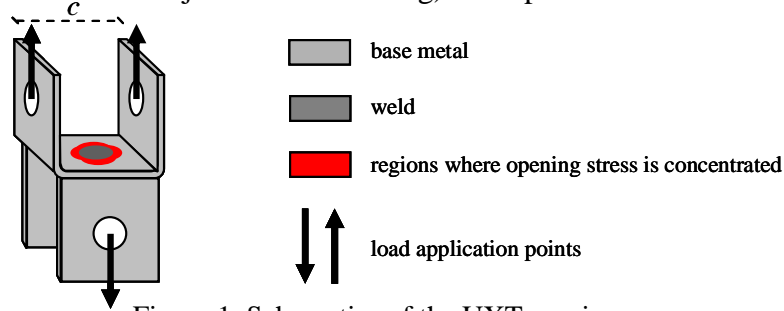


Figure 1. Schematics of the UXT specimen

Table 1. Chemical composition and mechanical properties of the three base material sheets

Material	C [wt%]	Mn [wt%]	Si [wt%]	0.2% proof stress [MPa]	Tensile strength [MPa]	Uniform elongation [%]
Steel F	0.15	0.68	0.01	380	505	14
Steel D	0.15	1.90	0.21	510	780	14
Steel T	0.19	1.71	1.68	540	820	22

Table 2. Welding conditions, room temperature properties and microstructure of the welds

Base metal	Welding current (kA)	d (mm)	CTS (kN)	HV <sub>0.5</sub> (base metal)	HV <sub>0.5</sub> (nugget)	Nugget microstructure
Steel F	7.6	6.2 ± 0.1	6.3 ± 0.1	160 ± 6	373 ± 30	martensite + lower bainite
Steel D	6.8	5.9 ± 0.1	7.2 ± 0.6	243 ± 3	420 ± 11	martensite
Steel T	7.0	6.4 ± 0.2	7.5 ± 0.1	243 ± 9	500 ± 10	martensite

## 2.2. Ductile to brittle transition curves of the weld nuggets

Specimen halves (full thickness 30x95 mm<sup>2</sup> coupons) were press-brake bent into U shapes with a bending radius of 2 mm, leaving a 30x30 mm<sup>2</sup> central region, and then welded perpendicularly to each other (Fig. 1). The specimen was attached to grips by bolts, with spacers inserted between specimen and bolts. The weld was thus loaded normally to the sheet plane. This setup was fitted to an Instron servohydraulic tensile machine, with a 250 kN load cell and a climatic chamber. Temperature was recorded using a thermocouple spot-welded on the UXT specimen. The tensile load and load line displacement curves were recorded, together with the increase in potential drop. The stress intensity factor was estimated using the analytical formula developed by Lin and Pan for square-cup specimens [4] (Eq. 1) over the first 2 mm of crack propagation:

$$K_I = \frac{\sqrt{3}T}{2\pi^{3/2}} \left\{ \frac{f_c c^2 [d^2 - c^2 + 2d^2 \ln(c/d)]}{Y(d^2 - c^2)} - \frac{(d^2 - c^2)(-1 + \nu) + 2c^2(1 + \nu) \ln(c/d)}{d^2(-1 + \nu) - c^2(1 + \nu)} \right\} \quad (1)$$

In Eq. (1),  $c$  is the cup diameter (taken as equal to  $c'$ , the equivalent diameter of the U tensile specimen),  $t$  the sheet thickness,  $d$  the weld diameter and  $T$  the tensile load.  $Y = d^2(\nu - 1) - c^2(\nu + 1)$ ,  $\nu = 0.3$  (Poisson ratio) and  $f_c$  is a geometrical parameter set to 1. Ductile-to-brittle transition (DBT) curves were determined using the fracture toughness at crack initiation,  $K_{Ic}$  (in fact, crack propagation leading to a reduction of the bearing area by 2%). Ductile and brittle temperature ranges were estimated from fracture surface examinations by scanning electron microscopy in a secondary electron imaging mode. Energy dispersive spectrometry (EDS) was used to analyse particles on fracture surfaces.

## 2.3. Plastic yield and fracture properties of the weld nugget

Two approaches have been reported in literature to estimate the constitutive behaviour of the nugget: using miniature specimens machined from “actual” nuggets (e.g. [5]), or simulating the coarse-grained heat-affected zone by heat treatment (e.g. [1]). The second approach was chosen here. Using a Gleeble 3500 simulator under a vacuum, full-thickness 12x100 mm<sup>2</sup> blanks were heated at 1500°C.s<sup>-1</sup> up to 1290°C (maximum heating rate and temperature that ensured homogeneous heating without local melting), and then cooled using helium gas blowing or water spraying (the actual spot welding cooling rate lying in between). From temperature monitoring with spot-welded thermocouples and microhardness measurements, a homogeneous heat treatment was applied over a length of at least 20 mm. Flat uniaxial tensile specimens (15x4 mm<sup>2</sup> in gauge dimensions) were spark erosion machined from heat-treated blanks and pulled in tension using the same Instron equipment at various temperatures, with an elongation rate of 1.1 10<sup>-3</sup> s<sup>-1</sup>, as measured from an *in situ* extensometer (initial gauge length: 8.7 mm). The criterion for small scale yielding (SSY) conditions in the UXT test was derived from these tensile properties. Double edge U-notched tensile (DENT) specimens were machined from heat-treated blanks of Steel D with a ligament width of 6 mm, a notch radius of 1 mm, and then pulled in tension using the same machine. Notch opening was recorded by averaging measurements of two extensometers placed at either edge.

## 3. Experimental results and discussion

### 3.1. Ductile to brittle transition curves of the weld nuggets

#### 3.1.1. Steel T

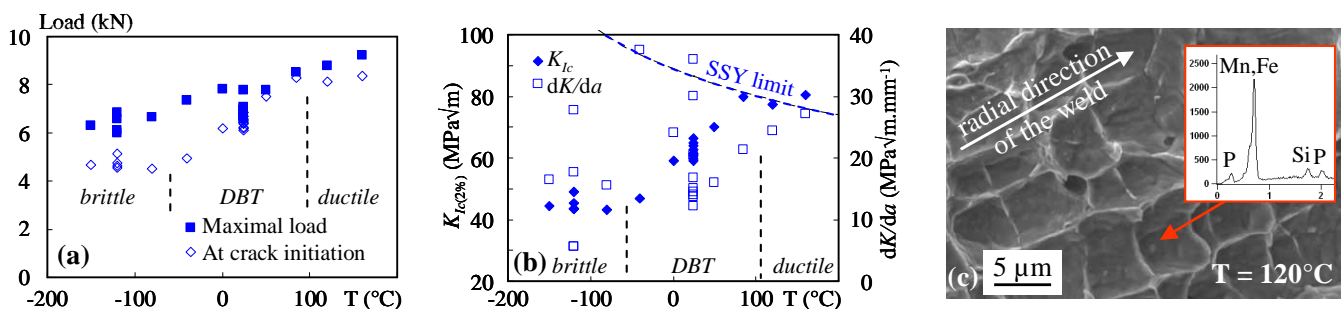


Figure 2. DBT curves for Steel T nuggets: (a) load at crack initiation and weld strength (i.e. maximal load); (b) fracture toughness at crack initiation and crack-extension resistance  $dK/da$ . c) Detailed view of ductile fracture and EDS analysis of precipitates located within dimples (red arrow)

Only interfacial failure (FIF) was observed. While the weld strength only slightly increases with temperature, a transition is observed in the load at crack initiation vs. temperature curve (Fig. 2). Above room temperature, the load only slightly increases between crack initiation and fracture. The fracture toughness transition curve showed a marked transition from 40-50 MPa√m up to 70-80 MPa√m. In the brittle temperature range, pure cleavage fracture initiated from multiple sites all around the weld. The microstructural feature at the origin of crack initiation could not be determined. Many crack deviations led to a rough fracture surface and to serrations in the load vs. displacement curves. In the ductile domain, smooth interfacial cracking occurred. Small dimples (~5 μm in size) aligned along the radial direction of the weld initiated from tiny particles of 0.4 μm in average size (Fig. 2c) that were mainly phosphides and sometimes aluminium oxides. The dimple size was consistent with the secondary dendrite arm spacing of the weld estimated from metallographic observations [6]. In the DBT range, cracks propagated in a mixed cleavage + ductile

manner. The roughness of the fracture surface decreased with increasing test temperature.

### 3.1.2. Steel D

Although some welds failed in a partial interfacial mode, FIF was observed in the vast majority of tests. The transition in crack initiation and fracture load is less obvious and more scattered than for Steel T but, again, the DBT range encompasses room temperature (Fig. 3). The fracture toughness in the brittle domain is similar to that of Steel T but in the ductile domain, it is lower. Cleavage and dimple ductile fracture exhibit similar macroscopic (crack deviation) and microscopic features as for Steel T. No particle was found at cleavage initiation sites. The average size of dimples and tiny particles (mainly MnS particles together with some phosphides) was 4.5 and 0.3  $\mu\text{m}$ , respectively.

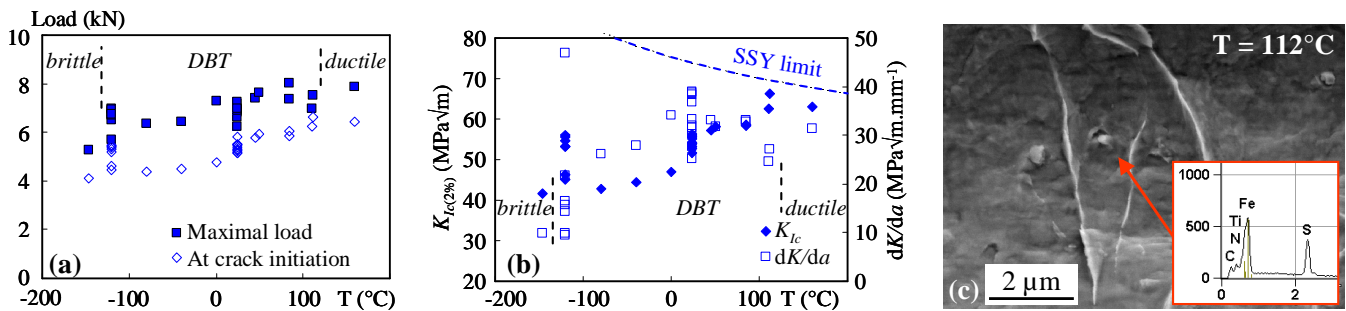


Figure 3. DBT curves for Steel D nugget: (a) load at crack initiation and weld strength; (b) fracture toughness at crack initiation and crack-extension resistance. (c) Ductile dimples nucleated at sulphides

### 3.1.3. Steel F

Only FIF was observed for Steel F. The load at crack initiation and the ultimate load increase with temperature up to  $0^\circ\text{C}$  and  $-100^\circ\text{C}$  respectively, and then decrease (Fig. 4). The fracture toughness varies in the same way as the load at crack initiation. In contrast to Steels T and D, only ductile fracture was observed at room temperature, yet with limited fracture toughness ( $\sim 55 \text{ MPa}\sqrt{\text{m}}$ ). The fracture mechanisms were similar to those of Steels T and D, with a dimple size of  $\sim 4 \mu\text{m}$  and a fine precipitation of MnS particles of  $\sim 0.5 \mu\text{m}$  in size together with a few aluminium oxides. Only a few cleavage facets were found at  $0^\circ\text{C}$  but cleavage facets linked by torn ligaments dominated fracture surfaces at  $-40^\circ\text{C}$ . Combined with transition curves, it suggests that cleavage and ductile fracture toughness could be very close to each other in this particular case.

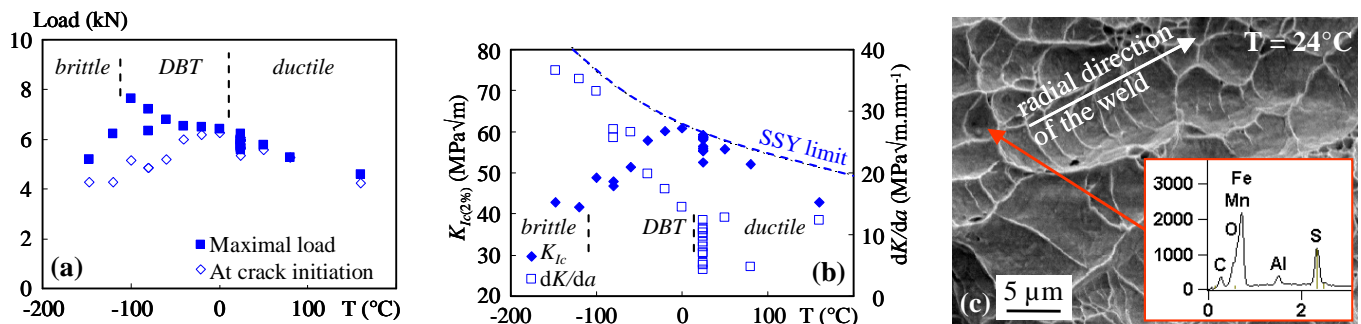


Figure 4. DBT curves for Steel F nugget: (a) load at crack initiation and maximal load; (b) fracture toughness at crack initiation and crack-extension resistance. (c) Ductile dimples nucleated at sulphides

### 3.1.4. Comparison between Steels T, D, and F

Despite their difference in fracture mechanisms, Steels F and D exhibit similar weld fracture

toughness at room temperature. The main difference between these steels seems to be the fracture toughness in the ductile domain, which increases with nugget hardness. This is consistent with the similar fracture mechanisms, dimple and particle size for the three steel nuggets: for the investigated welding conditions and sheet thickness, only the yield strength, controlled by their microstructure after cooling, seems to influence their fracture toughness in the ductile regime. Strong fracture deviation was associated with cleavage dominated fracture. Crack initiation occurred perpendicular to the applied load, where Mode I dominates. Cleavage initiation sites found all around the weld suggest a rather uniform value of Mode I stress intensity factor for this test. As cleavage cracks have to deviate to propagate across high-angle boundaries, the influence of Mode II loading, which is not uniform around the weld, may increase during cleavage crack propagation. No correlation appears between crack extension resistance and fracture mechanism (Figs 2b, 3b, 4b).

### 3.2. Tensile properties of simulated nugget microstructures

#### 3.2.1. Tensile properties of smooth specimens

The dependence of yield strength,  $YS$ , on temperature was satisfactorily modelled (Fig. 5) using a Zener-Hollomon equation (Eq. 2), with  $T$  the absolute temperature and  $\dot{\epsilon}$  the elongation rate:

$$YS = 10^a \left[ T \log_{10} \left( \frac{10^8}{\dot{\epsilon}} \right) \right]^b. \quad (2)$$

For Steels D and T, tensile properties are not very sensitive to cooling conditions (Table 3) due to the higher hardenability of these steels leading to auto-tempered martensite. The mechanical properties of the nugget were assumed to be similar to those of the helium-blown samples. Since the hardness and microstructure of Steel F nugget are intermediate between those of the martensitic water-sprayed and bainitic helium-blown samples, a “fictitious” material was considered in order to represent Steel F nugget: its mechanical properties and constitutive parameters were thus estimated from those of water-sprayed and helium-blown materials balanced by their respective hardness.

Table 3. Mechanical properties of heat-treated microstructure, nugget (edge) and “fictitious” material used to represent steel F nugget.  $Z$  is the reduction of area at fracture;  $a$  and  $b$  refer to Eq. 2

Steel	Cooling	Hardness (HV0.5)	0.2% proof stress (MPa)	Tensile strength (MPa)	Fracture elongation (%)	$Z$ (%)	$a$	$b$
T	Helium-blown	511 ± 9	1061	1547	19	45	4.19	-0.33
	Water-sprayed	548 ± 12	1086	1666	18	46	4.21	-0.33
D	Helium-blown	436 ± 11	932	1345	17	48	3.77	-0.23
	Water-sprayed	478 ± 8	1008	1443	17	49	4.26	-0.37
F	Helium-blown	296 ± 8	678	978	15	40	4.23	-0.41
	Water-sprayed	451 ± 9	862	1351	7	47	4.39	-0.41
	“Fictitious”						4.31	-0.41

#### 3.2.2. Tensile properties of notched Steel D specimens

As ductile fracture of the nugget is influenced by fine particles inherited from rapid solidification, heat-treated specimens were not representative of the nugget microstructure concerning ductile fracture. They were only used to derive an estimate of the critical stress necessary to initiate cleavage cracking. Five specimens were tested at -100°C, close to the brittle domain of Steel D nugget. Load vs. notch opening displacement curves presented a small serration around 18 kN, (Point B in Fig. 6a), well before final fracture. This could indicate brittle fracture initiation; no interrupted tensile test was available to prove this. Fracture surfaces (Fig. 6c) exhibited cleavage facets surrounded by ductile shear lips. Close to notch roots, cleavage facets are about 100-200 µm in size, similar to the prior austenite grain size of both helium-blown and nugget edge materials.

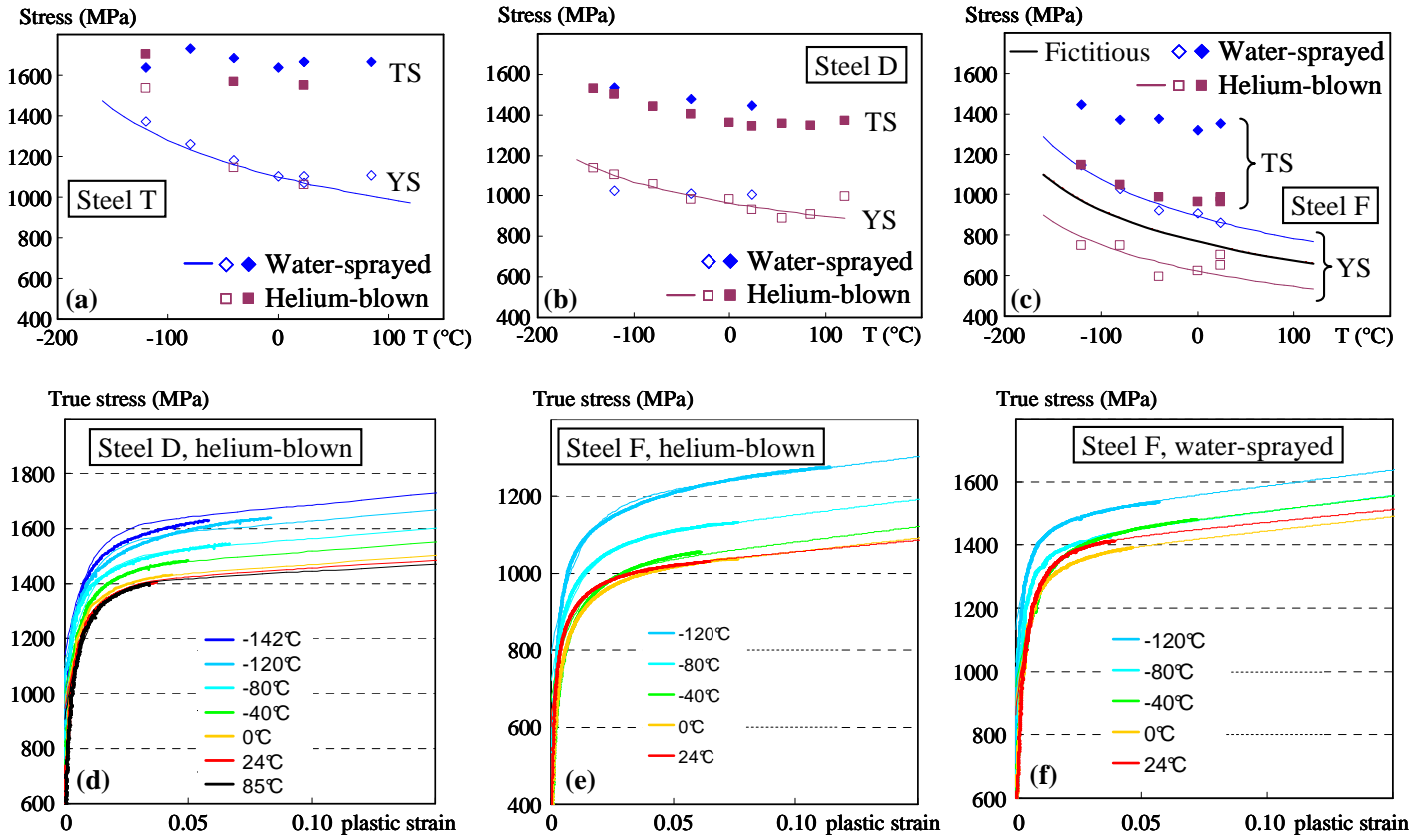


Figure 5. (a-c) Yield strength (YS), Zener-Hollomon fit (lines), and tensile strength (TS) of heat-treated steels. (d-f): Tensile curves: experiments (up to necking, thick lines) and model predictions (thin lines)

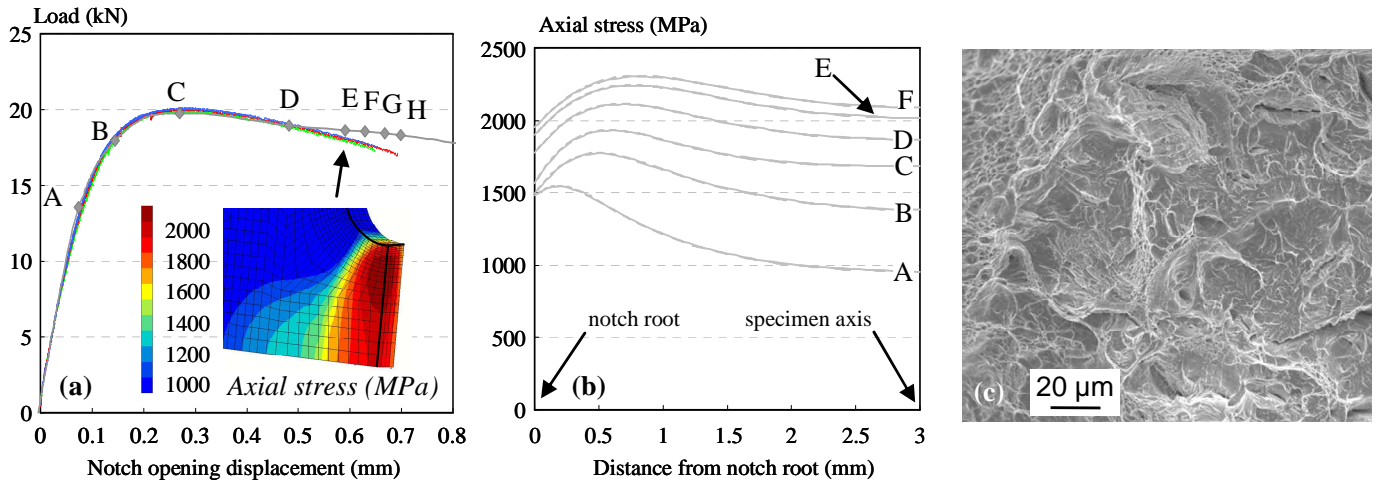


Figure 6. (a) Load vs. notch opening curves, (b) calculated axial stress along the ligament, and (c) fracture surface close to notch root of DENT specimens of helium-blown Steel D tested at -100°C

## 4. Mechanical analysis and derivation of a fracture criterion

### 4.1. Constitutive equations

Constitutive equations were determined from uniaxial tensile tests. The material were considered as elastic-plastic, homogeneous and isotropic, with Young's modulus  $E = 210,000$  MPa, and Poisson ratio  $\nu = 0.3$ . A von Mises yield criterion was used with a combined linear + Voce-like isotropic strain hardening equation, which reads as follows in the particular case of uniaxial tension:



$$\sigma_{eq} = \sigma_y + H\varepsilon_p + \sigma_y Q_1 (1 - \exp^{-b_1 \varepsilon_p}) + \sigma_y Q_2 (1 - \exp^{-b_2 \varepsilon_p}) \quad (3)$$

with  $\sigma_{eq}$  the von Mises equivalent stress,  $\sigma_y$  the yield strength,  $H$  a linear strain-hardening parameter mainly used for large amounts of strain,  $Q_1$ ,  $Q_2$ ,  $b_1$  and  $b_2$  being material parameters. According to the shape of experimental tensile curves, the values of  $Q_1$  and  $b_1$  were kept independent of temperature. The values of  $\sigma_y$ ,  $H$ ,  $Q_2$  and  $b_2$  were fitted for each temperature. Parameter  $H$  was determined from the constitutive equation [5] of a material similar to Steel D. This yields a value of e.g. 600 MPa at 24°C. The fitted sets of constitutive parameters very satisfactorily described tensile curves (Fig. 5d-f).

## 4.2. Cleavage crack initiation criterion from mechanical analysis of the DENT specimens

The mechanical analysis of the test was performed in three dimensions thanks to the in-house Z-set finite element software. One-eighth of the specimen was meshed with quadratic bricks with reduced integration. The specimen head and the region close to the notch were respectively attributed constitutive parameters of base metal and of the helium-blown material. Displacement of the specimen head was prescribed as in experiments. The simulated load vs. notch opening curve fits well with experimental results up to a notch opening of ~0.5 mm (Fig. 6a). The axial stress reaches its maximum ( $\sigma_{c,p} = 1790 \pm 40$  MPa) at 0.5 mm from the notch root at the onset of experimentally observed serrations, and ( $\sigma_{c,f} = 2270 \pm 20$  MPa) at 0.8 mm from the notch root for notch opening corresponding to experimental fracture (Points E-H in Figs 6a and 6b).

## 4.3. Simplified finite element modelling of the U-shape cross-tensile test

### 4.3.1. Modelling the UXT test

Only the upper part of the specimen was modelled, with usual symmetry conditions. Instead of a U-shaped cross tensile specimen, involving full 3D modelling, a circular-cup geometry was selected and represented by an axisymmetrical model (Fig. 7a). Consequently, the crack is only loaded in Mode I, which can induce dissimilarities with UXT tests especially during crack propagation but here, only crack initiation was considered. The finite element analysis software Abaqus/Implicit Standard was used with CAX4R elements (4-node bilinear axisymmetrical quadrangles with reduced integration and hourglass control). The following simplifying assumptions were made:

- Indentations caused by the electrodes, located far from the notch tip were not taken into account. The spacer inserted in the U specimen was not meshed but taken into account by allowing no displacement along the horizontal axis of the inner side of the flange.
- The ligament was only composed of the nugget section, i.e. the initial crack included both the non-welded interface and the DBZ. The nugget and harder part of the heat-affected zone was assimilated to the nugget material, the softer part of the heat-affected zone being assimilated to the base metal. The boundary between these two regions was taken perpendicular to the interface and located at 0.8 mm from the crack tip.
- Prescribed displacement was applied to a spring on the specimen flange which represents the stiffness of the load line [1]. The load is the resultant force on the spring. The stiffness of the spring ( $25 \text{ kN.mm}^{-1}$ ) was fitted to the linear part of the load vs. displacement curves. To this aim, the shift in displacement observed at low loads, probably due to some clearance compensations at the beginning of the tests, were ignored (Fig. 7b).
- To ensure an accurate description of the stress and strain fields around the crack tip, an initial semi-circular blunting was modelled. Taking typical values of  $K_I$  ( $60 \text{ MPa}\sqrt{\text{m}}$ ) and  $\sigma_y$  (1000 MPa) leads to a crack tip opening displacement of about 17  $\mu\text{m}$  under a plane strain assumption.



Consequently, the initial crack tip radius was set to  $2\text{ }\mu\text{m}$  together with a mesh size close to  $0.5\text{ }\mu\text{m}$ . Although the weld strength is overestimated by the model (Fig. 7b) (presumably because of neglecting work-hardening in folded regions and/or of the axisymmetry hypothesis), modelling results have been used to estimate stress and strain fields in front of the crack tip.

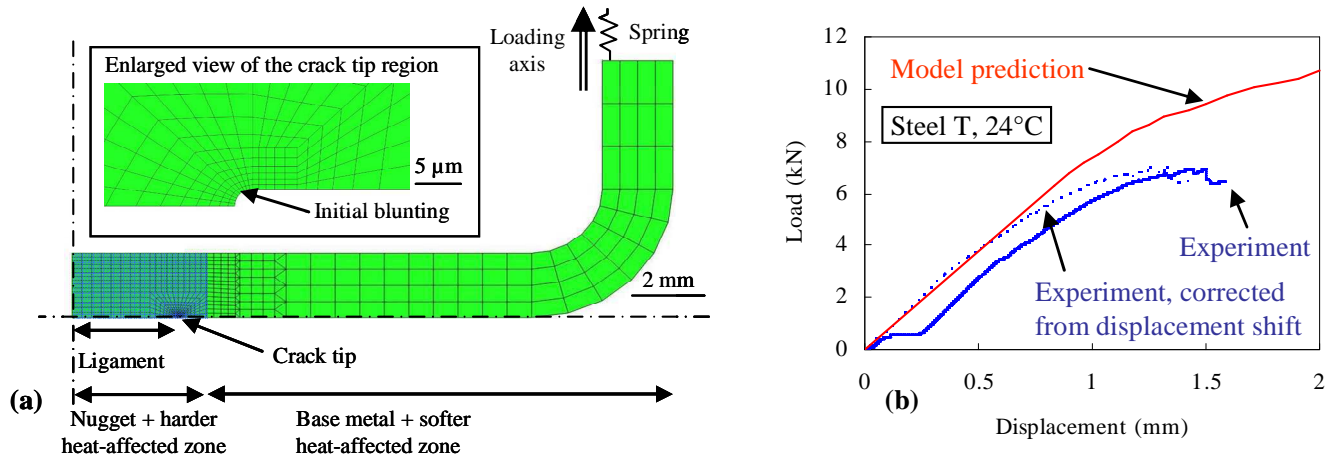


Figure 7. (a) Simplified finite element model and (b) experimental and simulated UXT load vs. displacement curves of Steel T

#### 4.3.2. Derivation of the stress intensity factor and energy release rate

The finite element model was validated by considering a fully elastic specimen. The difference between the predicted value of  $K_I$  and that derived from the Lin & Pan formula is only  $3\text{ MPa}\sqrt{\text{m}}$  for  $K_I = 60\text{ MPa}\sqrt{\text{m}}$ . As a consequence of the elastic-plastic behaviour of the material, the crack tip singularity was then described by the energy release rate, assimilated to the J-integral. The independence of calculated  $J$  with respect to the contour (chosen within the weld material, at least  $0.5\text{ mm}$  from the crack tip) was verified in the case of Steel T welds tested at room temperature.

#### 4.4. Assessment of a cleavage crack initiation criterion using the UXT test

The stress state in the nugget during the UXT test is described here by considering Steel D tested at room temperature (Fig. 8a-b). The central part of the nugget (up to  $2\text{ mm}$  from the weld centre) is loaded in compression. Positive values of opening stress are concentrated within a narrow region ( $0.6\text{--}0.8\text{ mm}$  in width) in front of the crack tip, leading to high values (up to  $4000\text{ MPa}$ ). The high radial stress, which can reach  $2500\text{ MPa}$ , was attributed to constraints induced by spacers: the base material is not only bent but also stretched along the sheet plane. The high resulting stress triaxiality limits plastic yielding in front of the crack tip. The opening stress ahead of the crack is represented in Fig. 8c for  $J = 9.9\text{ kJ.m}^{-2}$  (close to the fracture toughness at  $0^\circ\text{C}$ .) The opening stress depends on test temperature over  $50\text{ }\mu\text{m}$  ahead of the crack tip, i.e. in the plastically deformed region. For a given value of  $J$ , decreasing the test temperature tends to increase the maximal opening stress. The distance ( $\sim 15\text{ }\mu\text{m}$ ) at which the stress is highest is almost independent of test temperature.

The Ritchie-Knott-Rice (RKR) model [7] was tentatively applied (Fig. 8c). The region where the opening stress is higher than  $\sigma_{c,f}$  ( $\sigma_{c,f} = 2270\text{ MPa}$ ) is about  $70\text{ }\mu\text{m}$  in size for  $J \sim 10\text{ kJ.m}^{-2}$  whatever the test temperature. This is larger than the plastic zone size (about  $50\text{ }\mu\text{m}$ ). As plastic deformation is required to initiate cleavage cracking, crack initiation could be controlled by the extent of the plastic zone rather than by that of the region where the maximum principal stress exceeds its critical value. Cleavage fracture is thus not well described using such a simple approach. A statistical model based on the weakest link like that of Beremin [8] would probably be more appropriate.

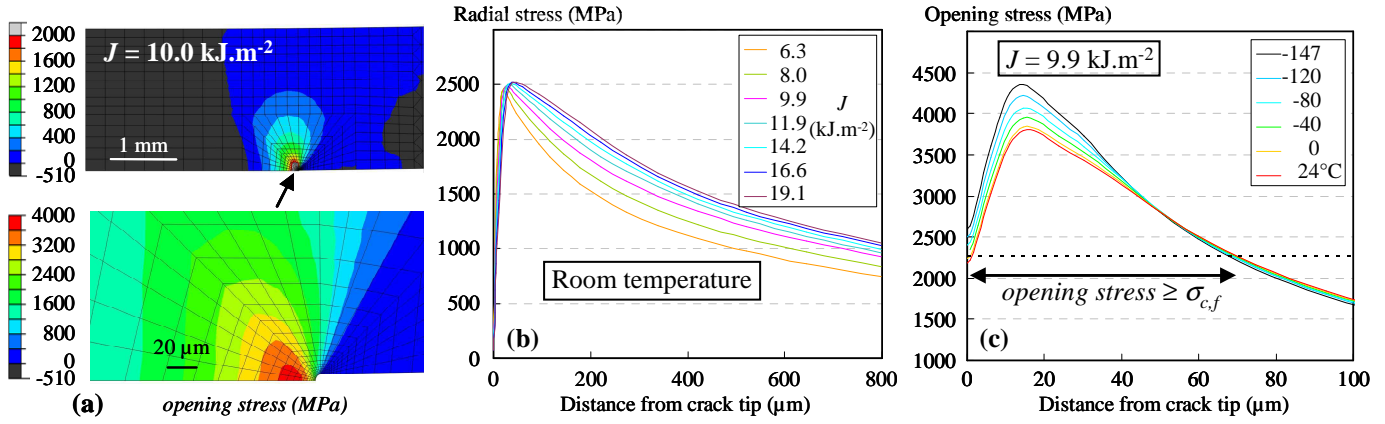


Figure 8. Model predictions of (a) opening stress field at room temperature in the weld, (b) radial stress along the interface as a function of  $J$  and (c) opening stress profile as a function of temperature for Steel D

#### 4.5. Assessment of a ductile fracture criterion using the UXT test

By using the Rice & Tracey model [9], the instantaneous void growth rate can be written as:

$$\frac{dR}{R} = \alpha \exp\left(\frac{3}{2}\tau\right) dp, \text{ leading to } \ln \frac{R}{R_0} = \int_{p_0}^p \alpha \exp\left(\frac{3}{2}\tau\right) dp \quad (4)$$

In Eq. 4,  $R$  is the void radius ( $R_0$  is its initial value),  $\alpha = 0.283$ ,  $\tau$  is the stress triaxiality ratio,  $p$  is the equivalent plastic strain and  $p_0$  is the equivalent plastic strain at void nucleation. In the absence of interrupted UXT tests, the value of  $p_0$  was set to zero. Determination of the critical value  $(R/R_0)_c$  of  $R/R_0$  requires a microstructure representative of the fine particle-containing nugget and could thus only be fitted from the UXT tests. Macroscopic fracture, characterized by  $J = J_c$ , occurs as soon as the local criterion  $R/R_0 = (R/R_0)_c$  is satisfied over a critical distance  $d_c$  ahead of the crack tip. This critical distance is usually close to a typical distance involved in the fracture process: the initial void spacing for instance. It was arbitrarily set to  $d_c = 8 \mu\text{m}$ , i.e., two times the void spacing observed in fracture surfaces (Fig. 3c).

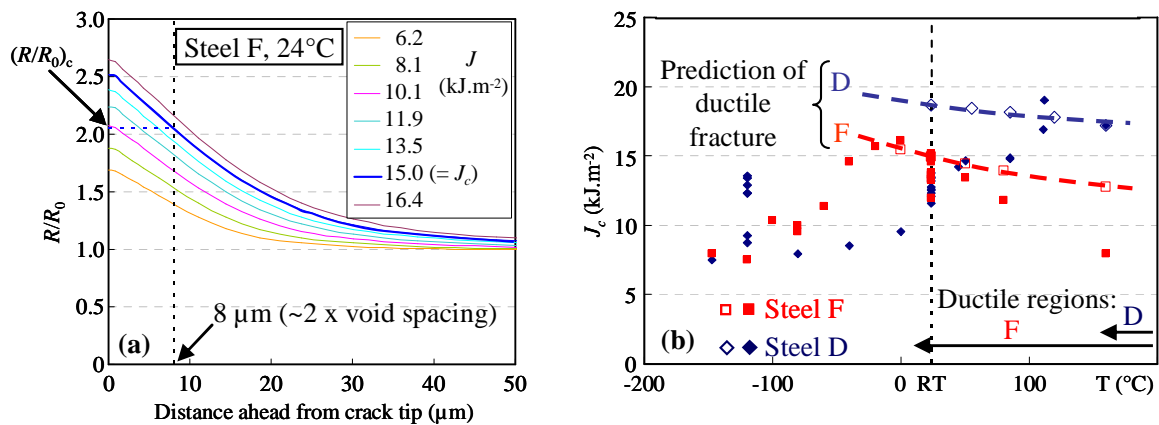


Figure 9. (a) Predicted void radius at room temperature and (b) comparison between experimental (full symbols) and predicted  $J_c$  (open symbols interpolated with lines) as a function of temperature

The Rice & Tracey model was first applied to ductile fracture of Steel F nugget at room temperature. The experimental fracture toughness of  $58 \text{ MPa}\sqrt{\text{m}}$  corresponds to  $J_c \sim 15 \text{ kJ.m}^{-2}$ , under a plane strain assumption. This value is reached when  $R/R_0$  exceeds 2.05 over  $d_c$  (Fig. 9a). The value of  $(R/R_0)_c$  is thus estimated to around 2.05. The void growth model was then applied to describe the evolution of

the fracture toughness in the ductile temperature range of Steel F and Steel D nuggets (Fig. 9b). The values of  $d_c$  were set to two times the initial void spacing and  $(R/R_0)_c = 2.05$  for the two materials. Void growth occurs much more rapidly with  $J$  when the temperature increases, due to the decrease in yield strength and strain hardening. Consequently, the values of the J-integral for which  $R/R_0 > (R/R_0)_c$  over distance  $d_c$  decrease with increasing temperature. The values of  $J_c$  calculated from the void growth model were compared to those experimentally determined thanks to the UXT tensile tests with a plane strain approximation to estimate  $J_c$  from  $K_{Ic}$  (Fig. 9b). For Steel F, the decrease in  $J_c$  in the ductile region is qualitatively predicted but the predicted fall of  $J_c$  at higher temperatures is underestimated. A possible source of discrepancy is the extrapolation of constitutive parameters for temperatures above 24°C. Model predictions are satisfactory for Steel D nugget at 120°C where ductile fracture prevails.

## 5. Conclusions

The U-shape cross-tensile (UXT) test was applied to the local approach of fracture of high strength steel resistance spot welds. A ductile-to-brittle transition curve was obtained for the three steels. For two of them, the transition encompasses room temperature.

- Brittle fracture occurred by cleavage cracking. The critical cleavage initiation stress was estimated to around 2270 MPa. The lower the temperature, the higher the tendency to crack deviation in the UXT test, leading to macroscopic fracture toughness that could reach that obtained in ductile fracture ( $\sim 60 \text{ MPa}\sqrt{\text{m}}$ ). The complex stress state in the UXT test combines in-plane tension and bending ahead of the crack tip. This reduces the size of the plastic zone; a simple approach such as the RKR model is not applicable.
- Ductile voids initiate from a dense distribution of fine sulphide or phosphide precipitates that result from rapid solidification of the weld. The high stress triaxiality and the small distance between voids lead to rapid interfacial crack propagation without crack deviation. This behaviour was quantitatively related to microstructural features using a Rice and Tracey approach.

## References

- [1] S. Dancette, D. Fabrègue, V. Massardier, J. Merlin, T. Dupuy, M. Bouzekri, Experimental and modelling investigation of the failure resistance of Advanced High Strength Steels spot welds. *Eng Fract Mech*, 78 (2011) 2259-2272.
- [2] Y.J. Chao, Failure mode of spot welds: interfacial versus pullout. *Sci. Technol. Welding Joining*, 8 (2003) 133-137.
- [3] F. Krajcarz, A.F. Gourgues-Lorenzon, E. Lucas, A. Pineau, Fracture toughness of the molten zone of resistance spot welds, submitted to *Int J Fract* (January, 2013)
- [4] P.C. Lin, J. Pan, Closed-form structural stress and stress intensity factor solutions for spot welds in commonly used specimens. *Eng Fract Mech*, 75 (2008) 5187-5206.
- [5] R. Lacroix, A. Lens, G. Kermouche, J.M. Bergheau, H. Klöcker, Local mechanical characterisation of a resistance spot weld of advanced high strength steel, in: *Proc. 19th French Congress of Mechanics, AFM, Courbevoie, 2011* (in French) <http://hdl.handle.net/2042/37135>.
- [6] F. Krajcarz, A. F. Gourgues, V. Bochard, E. Lucas, M. Bobadilla, Development and solidification of the molten zone of resistance spot welds : influence of welding parameters, in : *Matériaux 2010*, paper 1211 (2010) (in French) <http://hal-ensmp.archives-ouvertes.fr/hal-00570567>.
- [7] R.O. Ritchie, J. Knott, J.R. Rice, On the relationship between critical tensile stress and fracture toughness in mild steel, *J Mech Phys Solids*, 21 (1973) 395-410.
- [8] F.M. Beremin, A local criterion for cleavage fracture of a nuclear pressure vessel steel. *Metall Trans A*, 14 (1983) 2277-2287.
- [9] J.R. Rice, D.M. Tracey, On the ductile enlargement of voids in triaxial stress fields, *J Mech Phys Solids*, 17 (1969) 201-217.